photonics

MDPI

Article

Design and Diffraction Efficiency Analysis of Field-of-View Deflectors Using Self-Achromatic Grism

Na Xie [1,2], Jingyi Fu [2], Yunan Wu [1], Bingqing Xie [1], Ning Ma [1] and Jun Chang [1,*]

[1] National Key Laboratory on Near-Surface Detection, School of Optics and Photonics, Beijing Institute of Technology, Beijing 100081, China; 3120245397@bit.edu.cn (N.X.); 3120235112@bit.edu.cn (Y.W.); 3120235116@bit.edu.cn (B.X.); 3120245379@bit.edu.cn (N.M.)

[2] National Key Laboratory of Electromagnetic Space Security, Tianjin 300308, China; fujingyi0127@163.com

* Correspondence: optics_chang@126.com

Abstract

Field-deflection optical elements play a significant role in various high-resolution and field-of-view (FOV) expandable optical systems. In our previous work, we proposed a self-achromatic double-faced grism (DFG) configuration capable of field deflection. In this paper, to effectively guide the design and fabrication of DFG diffractive microstructures, we analyze the diffraction process of light within the DFG based on scalar diffraction theory, establish a diffraction efficiency model for the DFG, and propose an optimization method to improve diffraction efficiency over all FOVs while minimizing diffraction efficiency variations across the waveband. Following this design approach, two DFGs for 3–5 μm were specifically designed: one for a 4.4° FOV with 1.6° deflection, and the other for a 40° FOV with 15° deflection. Further optimization increased the bandwidth-integrated average diffraction efficiency (BIADE) to above 0.93 and reduced the diffraction efficiency variations across the waveband by 23.5% and 48%. And based on a tolerance analysis model, we performed tolerance analysis of the designed DFGs. The BIADE of both elements across all FOVs can exceed 0.86 after adding fabrication errors, maintaining a high diffraction efficiency. The results demonstrate that this method can effectively guide the design and manufacturing of diffractive microstructures.

Keywords: diffraction; field deflection; double-faced grism; diffractive microstructure

1. Introduction

With the continuous emergence and practical application of various new technologies, the performance requirements for imaging systems have become increasingly demanding, including larger FOVs and higher resolution. A long-standing challenge in imaging system design is the expansion of large FOVs, in which field-deflecting optical elements play a critical role. To reduce the overall system size and power consumption, the primary method for FOV expansion employs Risley prisms as field-deflection components, using electrically driven Risley prisms to steer the instantaneous FOV of the imaging optical system. This approach sequentially captures images from different sub-fields and subsequently stitches them into a panoramic image [1–3]. However, the major drawback of using Risley prisms as field-deflection elements is their inherent chromatic aberration, which manifests as lateral chromatic aberration and is difficult to compensate for using subsequent rotationally symmetric imaging optical systems. Therefore, the technical challenge of achieving self-achromatism limits their application in broadband imaging, restricting their use largely to monochromatic systems.

Check for updates

Received: 18 March 2026
Revised: 21 April 2026
Accepted: 23 April 2026
Published: 27 April 2026

Copyright: © 2026 by the authors. Licensee MDPI, Basel, Switzerland. This article is an open access article distributed under the terms and conditions of the Creative Commons Attribution (CC BY) license.

In recent years, technological innovations in diffractive optics have significantly enhanced the performance of classical optical design [4–7]. At the same time, they have provided more possibilities for addressing the chromatic aberration issue in Risley prisms. For instance, Chen proposed schemes combining achromatic prisms and apochromatic prisms with diffractive gratings [8,9]. Weber et al. fabricated etched diffractive gratings on the surface of a ZnSe prism and developed a dual-prism scanning system incorporating a diffraction correction module [10]. Prism–grating hybrid optical elements have been widely adopted due to their advantages of low dispersion and a compact structure [11–14]. However, due to the discrepancy between the dispersion of the diffraction surface and that of the optical material, the self-achromatic performance of this prism–grating structure is inferior when employed for FOV deflection in optical systems with small FOVs and large apertures. Nie Xin et al. further established a mathematical model for rotating dual-grating prisms [15]. To address the chromatic aberration under FOV deflection conditions, we previously proposed a self-achromatic double-faced grating–prism (DFG) structure based on a single prism [16]. This structure achieves self-achromatism through the mutual dispersion cancelation between the front and rear diffraction surfaces of the prism. Compared with the methods proposed by Chen and Weber, the achromatic configuration presented in this work can be applied to both narrow-FOV large-aperture and wide-FOV small-aperture optical systems for FOV deflection. Although the method for solving the self-achromatic parameters of the DFG (including apex angle, periods of the two diffractive surfaces, diffraction orders, and residual chromatic aberration) was presented in that paper, the study lacks investigations on the design method of the diffractive microstructures and the analysis of diffraction efficiency of the DFG, making it difficult to proceed directly to the actual fabrication stage.

Due to its characteristic dimensions being significantly larger than the incident light wavelength, the DFG can be effectively analyzed using scalar diffraction theory, which meets both design and accuracy requirements. Its structure closely resembles that of double-layer diffractive optical elements (DLDOEs), making the diffraction efficiency analysis and design methodologies of DLDOEs largely applicable as references. For instance, Xue [17,18] investigates and presents the mathematical relationship between diffraction efficiency and wavelength in DLDOEs, proposing a bandwidth-integrated average diffraction efficiency (BIADE) maximization method. Mao [19] introduces a microstructure height optimization method based on angle-bandwidth-integrated average diffraction efficiency, analyzing the impact of wavelength and field angle on the diffraction efficiency of DLDOEs. Due to significant variations in the diffraction efficiency of the diffractive surface at different wavelengths, the diffraction efficiency in certain bands can be severely reduced, thereby diminishing the detection capability of the optical detection system for targets with prominent radiation characteristics in those bands. To avoid this, it is necessary to minimize the differences in diffraction efficiency across the waveband.

In this paper, to promote the practical fabrication and application of the DFG, we analyze the diffraction process of light in the DFG based on scalar diffraction theory, establish a diffraction efficiency model for the DFG, and propose an optimization method to improve diffraction efficiency over all FOVs while minimizing diffraction efficiency variations across the waveband. Meanwhile, we have designed the diffractive microstructures for two DFGs using the proposed method and performed tolerance analysis on the design results. Section 2 introduces the diffraction efficiency model of the DFG, including the diffraction efficiency calculation model, diffraction efficiency optimization model, and tolerance analysis model. Sections 3 and 4 present the optimal design of diffractive microstructures for two types of DFGs, as well as the analysis of their diffraction efficiency and tolerance characteristics. Section 5 presents the discussion.

2. Design Theory of Diffractive Microstructures for DFG

2.1. Diffraction Efficiency Calculation Model

The configuration of the self-achromatic DFG we proposed in ref. [16] is shown in Figure 1a [16]. This configuration involves etching a grating surface on the front and rear surface of an optical prism, achieving self-achromatism through two iterations of grating diffraction, and adjusting the incident angle on the grating via the apex angle to achieve field deflection. The ray transmission process for achieving the field-deflection angle using the DFG is illustrated in Figure 1b [16].

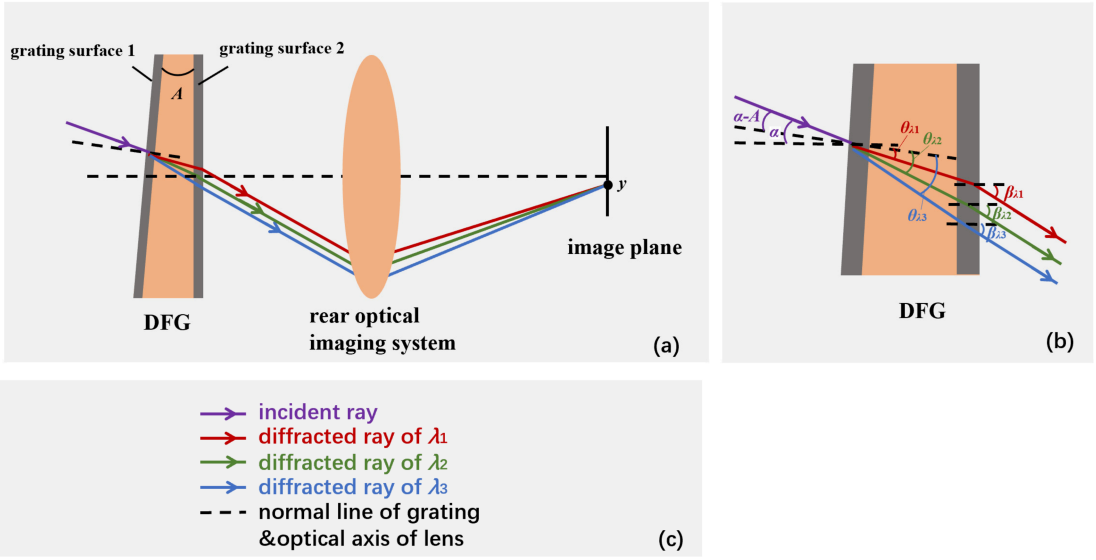


Figure 1. (**a**) The structure of a DFG and the process of ray deflection and focusing via a DFG. (**b**) Self-achromatism diffraction process upon passing through a DFG. The system operates over a waveband $\lambda_1 \sim \lambda_3$ centered at λ_2. The angles are defined as follows: FOV α; incident angle from Grating 1 $(\alpha - A)$; diffraction angles from Grating 1: $\theta_{\lambda1}, \theta_{\lambda2}, \theta_{\lambda3}$; corresponding diffraction angles from Grating 2: $\beta_{\lambda1}, \beta_{\lambda2}, \beta_{\lambda3}$; $\Delta\beta = \beta_{\lambda3} - \beta_{\lambda1}$. (**c**) Legend.

We designed the DFG using scalar diffraction theory, and the diffractive microstructures of the diffractive optical element are generally represented by multi-level phase gratings. Multi-level phase gratings have multi-step diffractive microstructures, and the diffraction efficiency gradually increases with the increase in the number of steps. For a DFG with an apex angle of A, the structure of its multi-level phase grating is shown in Figure 2, where the tooth height d is approximately equal to the sum of the heights Δ of the N-level microstructure, i.e., $d \approx N\Delta$.

When two light rays are obliquely incident on the DFG at an incident angle α (i.e., FOV), the phase difference generated on adjacent sub-periods can be expressed as

$$\varphi(\lambda) = \frac{1}{\lambda}\{[n_m(\lambda)y_1 - n_1(\lambda)y_2] + [n_2(\lambda)y_3 - n_m(\lambda)y_4]\} \quad (1)$$

where λ is the wavelength, $n_1(\lambda)$ is the refractive index of the incident medium, $n_m(\lambda)$ is the refractive index of the DFG substrate material, and $n_2(\lambda)$ is the refractive index of the exit medium. As shown in Figure 3, y_1 and y_2 represent the optical path difference in the rays on both sides of the first diffractive surface of the DFG, respectively; y_3 and y_4 represent the optical path difference in the rays on both sides of the second diffractive surface of the DFG.

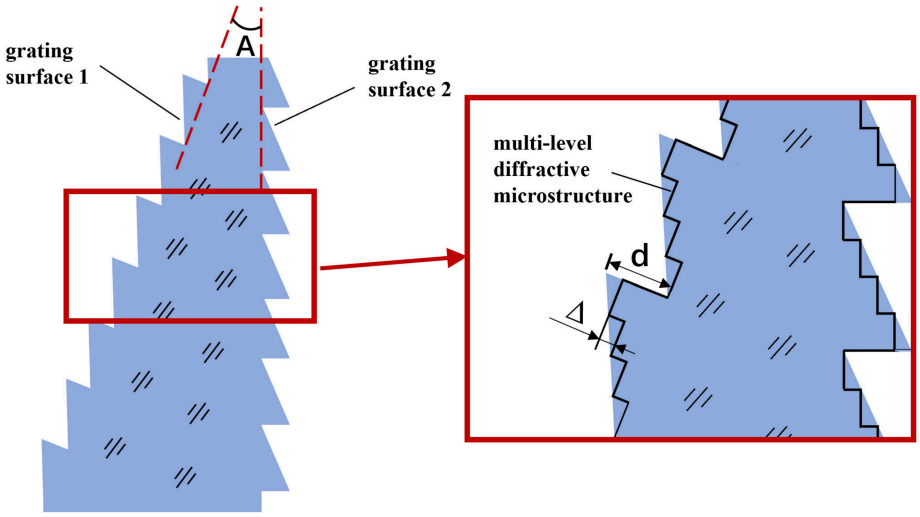


Figure 2. Schematic diagram of the DFG diffractive surface profile and its multi-level diffractive microstructure.

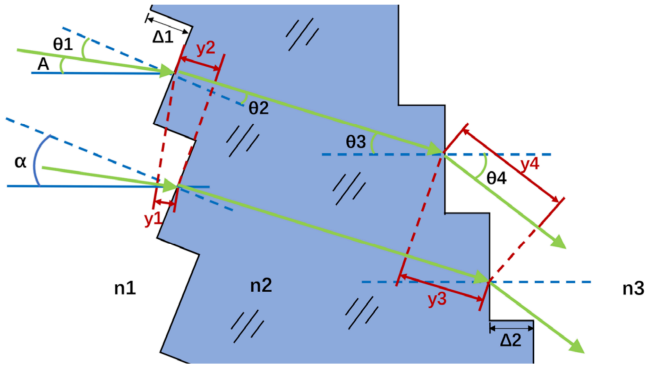


Figure 3. Situation of oblique incident light passing through adjacent sub-periods of the DFG. α is the current incident angle; A is the apex angle of DFG; θ_1, θ_2, θ_3 and θ_4 are the incident and exit angles at each diffractive surface when a light beam is diffracted by the DFG; $\theta_1 = \alpha + A$. We define the clockwise rotation angle of the light ray as "−" and the counterclockwise rotation angle as "+".

Similarly to the derivation of the diffraction efficiency for multi-level phase diffraction gratings, the phase delay expression for a sub-period of the DFG can be obtained from Equation (1) [20].

$$\begin{aligned}\varphi(\lambda) = \frac{\Delta_1}{\lambda}\left[\sqrt{{n_m}^2(\lambda) - {n_1}^2(\lambda)\sin^2(\alpha + A)} - n_1(\lambda)\cos(\alpha + A)\right] + \\ \frac{\Delta_2}{\lambda}\left[\sqrt{{n_2}^2(\lambda) - {n_1}^2(\lambda)\sin^2(\alpha + A)} - \sqrt{{n_m}^2(\lambda) - {n_1}^2(\lambda)\sin^2(\alpha + A)}\right]\end{aligned} \quad (2)$$

Then the phase delay of an N-level phase grating within one period T can be obtained as [20]

$$\phi(\lambda) = N\varphi(\lambda) \quad (3)$$

Let $N\Delta_1 = -N\Delta_2 \approx d_0$, where d_0 is the grating tooth height of the diffraction grating. Assume the diffraction order is m, the design wavelength is λ_0, and the design FOV is α_0. According to scalar diffraction theory [20], when $N \to \infty$, the tooth height d_0 can be determined using the diffraction efficiency formula for multilayer diffractive optical elements.

$$d_0 = m\lambda_0 / \left[\sqrt{{n_m}^2(\lambda_0) - {n_1}^2(\lambda_0)\sin^2(\alpha_0 + A)} \; - \; n_1(\lambda_0)\cos(\alpha_0 + A) \right.$$
$$\left. - \sqrt{{n_2}^2(\lambda_0) - {n_1}^2(\lambda_0)\sin^2(\alpha_0 + A)} - \sqrt{{n_m}^2(\lambda_0) - {n_1}^2(\lambda_0)\sin^2(\alpha_0 + A)} \right] \quad (4)$$

Substituting Equation (4) into Equations (2) and (3), the phase retardation at different wavelengths and different incident angles is

$$\phi(\lambda, \alpha) = \frac{d_0}{\lambda} \left[\sqrt{{n_m}^2(\lambda) - {n_1}^2(\lambda)\sin^2(\alpha + A)} \; - \; n_1(\lambda)\cos(\alpha + A) \right.$$
$$\left. - \sqrt{{n_2}^2(\lambda) - {n_1}^2(\lambda)\sin^2(\alpha + A)} - \sqrt{{n_m}^2(\lambda) - {n_1}^2(\lambda)\sin^2(\alpha + A)} \right] \quad (5)$$

According to the diffraction efficiency formula for diffractive optical elements, the diffraction efficiency equation for the DFG is [20]

$$\eta_m(\lambda) = \mathrm{sinc}^2[m - \phi(\lambda, \alpha)] \quad (6)$$

2.2. Diffraction Efficiency Optimization Model

According to Equations (3)–(6), the diffraction efficiency of the DFG can be further improved by optimizing the design wavelength λ_0, the design FOV α_0, and the diffraction grating tooth height d_0. Therefore, we take λ_0, α_0 and d_0 as optimization variables and obtain the optimal microstructure height d by designing a convergent objective function to enhance the diffraction efficiency of the DFG.

Usually, the bandwidth-integrated average diffraction efficiency (BIADE) is used to characterize the wide-band diffraction performance of diffractive optical elements. BIADE $\overline{\eta_m}$ is expressed as [17]

$$\overline{\eta_m} = \frac{1}{\lambda_{\max} - \lambda_{\min}} \int_{\lambda_{\min}}^{\lambda_{\max}} \eta_m(\lambda) d\lambda \quad (7)$$

where $\lambda_{\min}$ and $\lambda_{\max}$ represent the minimum and maximum wavelengths of the actual optical system, $\eta_m(\lambda)$ denotes the diffraction efficiency of the m-th order, and $\overline{\eta_m}$ is the BIADE of the DFG. A larger $\overline{\eta_m}$ indicates a higher diffraction efficiency of the element over a wide waveband.

Due to significant variations in the diffraction efficiency of the diffractive surface at different wavelengths, the diffraction efficiency in certain bands can be severely reduced, thereby diminishing the detection capability of the optical detection system for targets with prominent radiation characteristics in those bands. To avoid this, it is necessary to minimize the differences in diffraction efficiency across wavebands. Therefore, the standard deviation of waveband diffraction efficiency (SDWD) σ is introduced to evaluate the differences in diffraction efficiency at different wavelengths:

$$\sigma = \sqrt{\frac{\sum_{i=1}^{S} [\eta_m(\lambda_i) - \overline{\eta_m}]^2}{S - 1}} \quad (8)$$

where S is the number of wavelength samples within the design waveband and $\eta_m(\lambda_i)$ is the diffraction efficiency at the i-th wavelength.

Finally, to balance the improvement of $\overline{\eta_m}$ and the reduction of σ, the convergence objective function f is defined as

$$f = b\sigma + k(1 - \overline{\eta_m}) \tag{9}$$

where b and k are the weighting coefficients of σ and $\overline{\eta_m}$.

The optimization process of the DFG diffractive microstructure is shown in Figure 4. First, the initial values of the optimization variables λ_0, α_0, and d_0 were input based on the initial configuration of the DFG. Then, the optimization intervals $(\lambda_0 - \Delta\lambda, \lambda_0 + \Delta\lambda)$, $(\alpha_0 - \Delta\alpha, \alpha_0 + \Delta\alpha)$, and $(d_0 - \Delta d, d_0 + \Delta d)$ for the optimization variables were defined, where $\Delta\alpha$, Δd and $\Delta\lambda$ are user-defined interval differences. Subsequently, we used Equations (6) and (9) to calculate the minimum value of f for all optimization variables within their respective optimization intervals. Then, the corresponding tooth height d, designed incident angle α, and designed wavelength λ under this result could be determined by locating min(f). And these values of tooth height d, designed incident angle α, and designed wavelength λ are thus the optimized results. Finally, the double-sided height assignment of the DFG was completed (i.e., $d_1 = d$ and $d_2 = -d$), thus completing the optimization of the DFG diffractive microstructure.

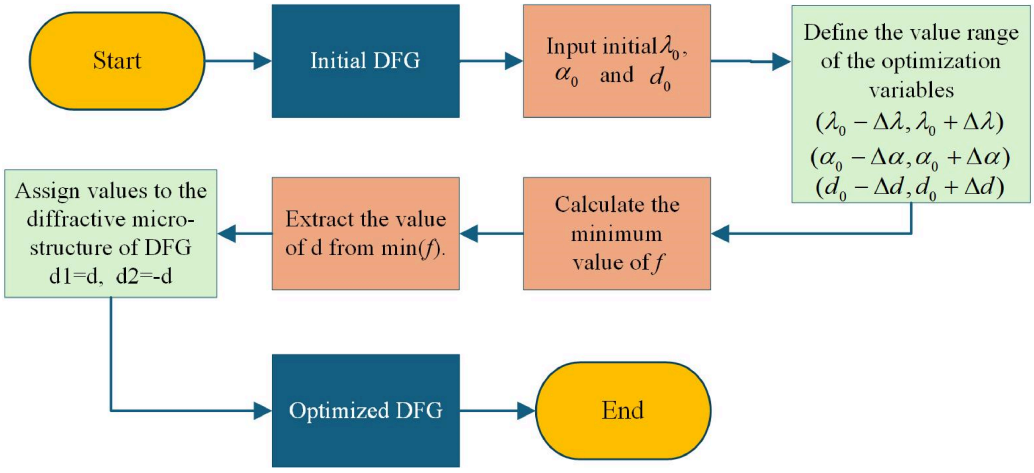


Figure 4. DFG optimization flowchart.

2.3. Tolerance Analysis Model

According to the structural characteristics of the DFG, we conducted a tolerance analysis of the DFG from the aspects of tooth height error, duty-cycle error, period error, and double-sided lateral alignment error.

As the tooth height corresponds to a submicron-scale microstructure, nanometer-precision control can be achieved via electron beam lithography (EBL), reactive ion etching (RIE), and other processes, and the repeatability and uniformity of the tooth height can be stably controlled within ±0.01 μm. In the fabrication of diffractive optical elements and gratings, the period positioning error can be confined to 1–5 μm by means of photolithography, laser direct writing, and precision alignment processes. The groove angle error can be regulated through precision lithography and alignment, with a general machining accuracy of ±0.1° to ±0.3°, which can be ensured by angle measurement and corrective machining. In photolithographic pattern transfer and etching, the control accuracy of linewidth and duty cycle typically reaches 3–5%.

a. Tooth height error (Δd_1 and Δd_2)

By adding tooth height error to the diffractive microstructures d_1 and d_2 on both sides

of the DFG, the diffraction efficiency calculation formula incorporating the error, based on Equations (4)–(6), is as follows:

$$\eta^*_{ma}(\lambda) = \sin c^2\left\{m - \frac{1}{\lambda}\left[(d_1+\Delta d_1)\left(\sqrt{{n_m}^2(\lambda) - {n_1}^2(\lambda)\sin^2(\alpha+A)} - n_1(\lambda)\cos(\alpha+A)\right)\right.\right.$$
$$\left.\left.+(d_2+\Delta d_2)\left(\sqrt{{n_2}^2(\lambda) - {n_1}^2(\lambda)\sin^2(\alpha+A)} - \sqrt{{n_m}^2(\lambda) - {n_1}^2(\lambda)\sin^2(\alpha+A)}\right)\right]\right\} \quad (10)$$

b. Duty-cycle error (Δf)
Generally, the duty cycle of the microstructure is set to 0.5. The further the duty cycle deviates from 0.5, the more significant the reduction in diffraction efficiency. The formula for diffraction efficiency introducing duty-cycle error is as follows:

$$\eta^*_{mb}(\lambda) = \eta_m(\lambda) \cdot \sin c^2\left\{1 - 4(\Delta f)^2\right\} \quad (11)$$

c. Period error (ΔT_1 and ΔT_2)
Period error refers to the fabrication error of the period on the two diffraction surfaces. The formula for diffraction efficiency with the introduction of period error is given by

$$\eta^*_{mc}(\lambda) = \eta_m(\lambda) \cdot \sin c^2\left\{1 + \frac{\Delta T_1}{T}\right\} \cdot \sin c^2\left\{1 + \frac{\Delta T_2}{T}\right\} \quad (12)$$

d. Double-sided lateral alignment error ($\Delta\Phi$ and Δy)
Double-sided lateral alignment error includes the relative rotation error of the two diffraction surfaces around the optical axis (i.e., the groove angle) $\Delta\Phi$ and the period alignment error Δy. The reduction in diffraction efficiency caused by the relative rotation error of the two diffraction surfaces around the optical axis is generally related to the beam diameter: the larger the angular error and the larger the beam diameter, the more significant the decrease in diffraction efficiency. The formula for diffraction efficiency introducing double-sided lateral alignment error is as follows:

$$\eta^*_{md}(\lambda) = \eta_m(\lambda) \cdot \sin c^2\left\{\frac{\pi D\Delta\phi}{2T}\right\} \cdot \sin c^2\left\{1 + \frac{\pi\Delta y}{T}\right\} \quad (13)$$

3. Narrow FOV Deflection Design Example

3.1. Diffractive Microstructure Design and Optimization

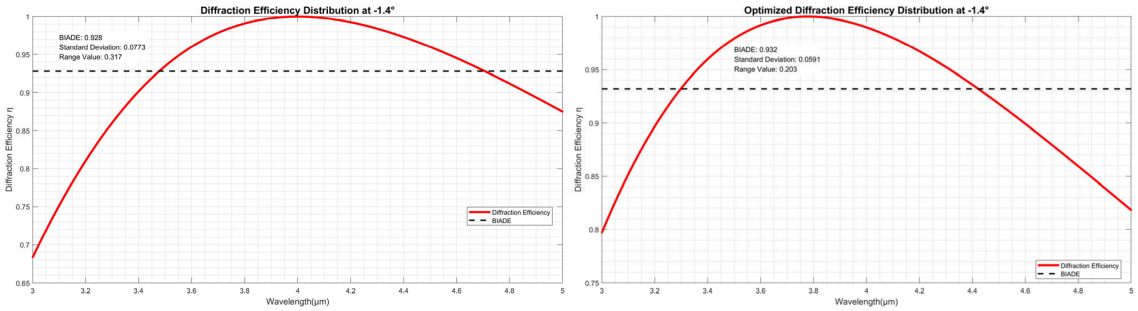
According to the design theory in Section 2, we have completed the optimal design of the DFG element in Ref. [16]. The initial FOV is ±2.2°, and the FOV after deflection ranges from −3.6° to +0.8°. Based on the optimization of the basic parameters of the DFG in Ref. [16], the design requirements of the decomposed element are listed in Table 1.

Table 1. Design requirements.

Parameters	Values
Substrate material	Silicon
Waveband (μm)	3~5
Beam diameter (mm)	37.5
Grating constant (mm)	0.131
Diffraction order	1
Apex angle (°)	0.4
FOV (°)	−3.6~+0.8
BIADE	>0.93
SDWD	<0.06

Based on the design requirements in Table 1, the initial design wavelength was determined to be 4 μm, the initial design FOV was −1.4°, the apex angle A = 0.4°, the diffraction order m = 1, and $n_1 = n_2 = 1$. The substrate material of the element was silicon, and according to the Cauchy dispersion formula for silicon, it was calculated as $n_m(\lambda_0) = 3.42$. Then, using Equation (3), the initial microstructure height d_0 was calculated to be 0.83 μm, so d_1 = 0.83 μm and d_2 = −0.83 μm. Based on Equations (4)–(6), the diffraction efficiencies at different FOVs and different wavelengths were calculated. Due to the small FOV span, there was almost no difference in the diffraction efficiency distribution across different FOVs.

Figure 5a shows the diffraction efficiency at different wavelengths for a FOV of −1.4°, where the minimum diffraction efficiency is 0.683 (λ = 3 μm) and the maximum diffraction efficiency is 1 (λ = 4 μm). It was calculated that $\overline{\eta_m}$ = 0.928, the range was 0.317, and σ = 0.0773.



(**a**) (**b**)

Figure 5. Diffraction efficiency at different wavelengths for the FOV of −1.4°. (**a**) Initial diffraction efficiency curve; (**b**) optimized diffraction efficiency curve.

Then we optimized the diffraction microstructure of the DFG using the optimization model presented in Section 2.2. In this optimization, the optimization interval for λ_0 was (3.8, 4.2), the optimization interval for α_0 was (−3, 0.2), and the optimization interval for d_0 was (0.75, 0.9). Here, the number of wavelength sampling points S was set to 100. In the convergence objective function f, b = 1 and k = 0.2. Before optimization, the value of the objective function was f = 0.092. After convergence optimization, it was reduced to f = 0.073, while the microstructure height was optimized to d = 0.78 μm with all other parameters remaining unchanged.

Figure 5b shows the optimized diffraction efficiency at different wavelengths for the FOV of −1.4°, where the minimum diffraction efficiency was 0.8 (λ = 3 μm) and the maximum diffraction efficiency was 1 (λ = 4 μm). It was calculated that $\overline{\eta_m}$ = 0.932, the range was 0.203, and σ = 0.0591. The range was reduced by 35%, and σ was reduced by 23.5%. After optimization, the performance of the DFG met the design requirements.

3.2. Tolerance Analysis

Based on several errors summarized in Section 2.3, we added manufacturing errors to the above DFG model. The error values and the corresponding field-averaged BIADE reduction effect are listed in Table 2.

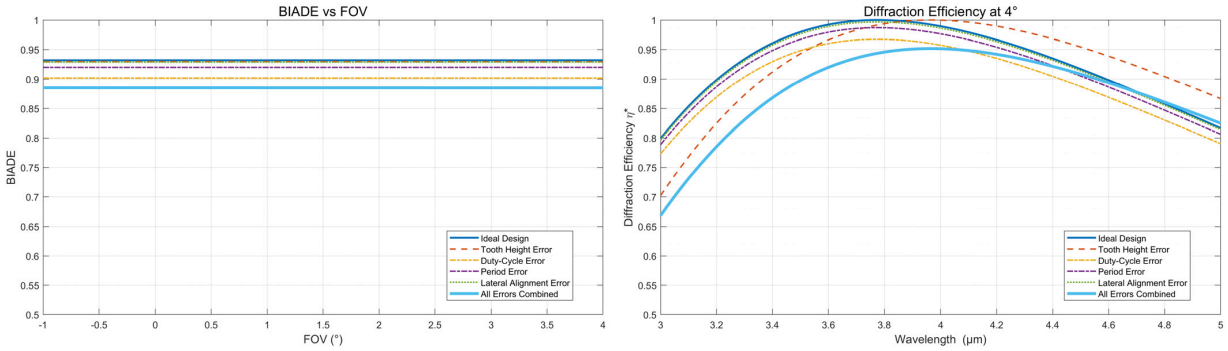
Table 2. Tolerance analysis results.

NO.	Error Name	Value	Loss of $\overline{\eta_m}$
1	Tooth height error	Δd_1 = 5% Δd_2 = 5%	0.24%
2	Duty-cycle error	Δf = 5%	3.25%

Table 2. *Cont.*

NO.	Error Name	Value	Loss of $\overline{\eta_m}$
3	Period error	$\Delta T_1 = 5\%$ $\Delta T_2 = -5\%$	1.29%
4	Double-sided lateral alignment error	$\Delta\Phi = 0.2°$ $\Delta y = 5\%$	0.33%
5	All errors combined		5.04%

The variation curves of BIADE with different errors for each FOV are shown in Figure 6a. The ideal BIADE for each FOV is 0.932, and it decreases to 0.882 after adding errors. The diffraction efficiency variation at different wavelengths after adding errors is shown in Figure 6b. The diffraction efficiency at each wavelength can reach more than 0.66.



(**a**) (**b**)

Figure 6. Tolerance analysis result. (**a**) BIADE with different errors for each FOV; (**b**) the diffraction efficiency variation at different wavelengths after adding errors.

Among them, the tooth height error is 0.04 μm and the period error is 5 μm, both of which can be achieved by existing processing technologies.

4. Wide FOV Deflection Design Example

4.1. Diffractive Microstructure Design and Optimization

To further analyze the diffraction efficiency performance of the DFG, we designed a DFG for wide FOV deflection using the method described in Ref. [16]. The initial FOV is ±20°, and the FOV after deflection ranges from −5° to +35°. The design requirements of the decomposed element are listed in Table 3.

Table 3. Design requirements.

Parameters	Values
Substrate material	Silicon
Waveband (μm)	3~5
Beam diameter (mm)	5
Grating constant (mm)	2.3
Diffraction order	1
Apex angle (°)	5
FOV (°)	−5~+35
BIADE	>0.93
SDWD	<0.08

According to the design requirements in Table 3, the initial design wavelength is determined as 4 μm, the initial design FOV is 15°, apex angle A = 5°, diffraction order m = 1, $n_1 = n_2 = 1$, and the substrate material of the element is silicon. The initial microstructure height d_0 = 0.81 μm is calculated according to Equation (3); thus, d_1 = 0.81 μm and $d_2 = -0.81$ μm. Based on Equations (4) and (5), the diffraction efficiency at different FOVs and different wavelengths is calculated and shown in Figure 7a. The BIADE at different FOVs calculated according to Equation (7) is shown in Figure 7c. Thus, it can be observed that the BIADE decreases with the increase in the FOV angle, where the maximum value is 0.931 at −5° and the minimum value is 0.904 at 35°. Figure 7e shows the diffraction efficiency at different wavelengths at 35°, where the minimum diffraction efficiency is 0.551, the maximum diffraction efficiency is 1, the range is 0.452, and σ = 0.1217.

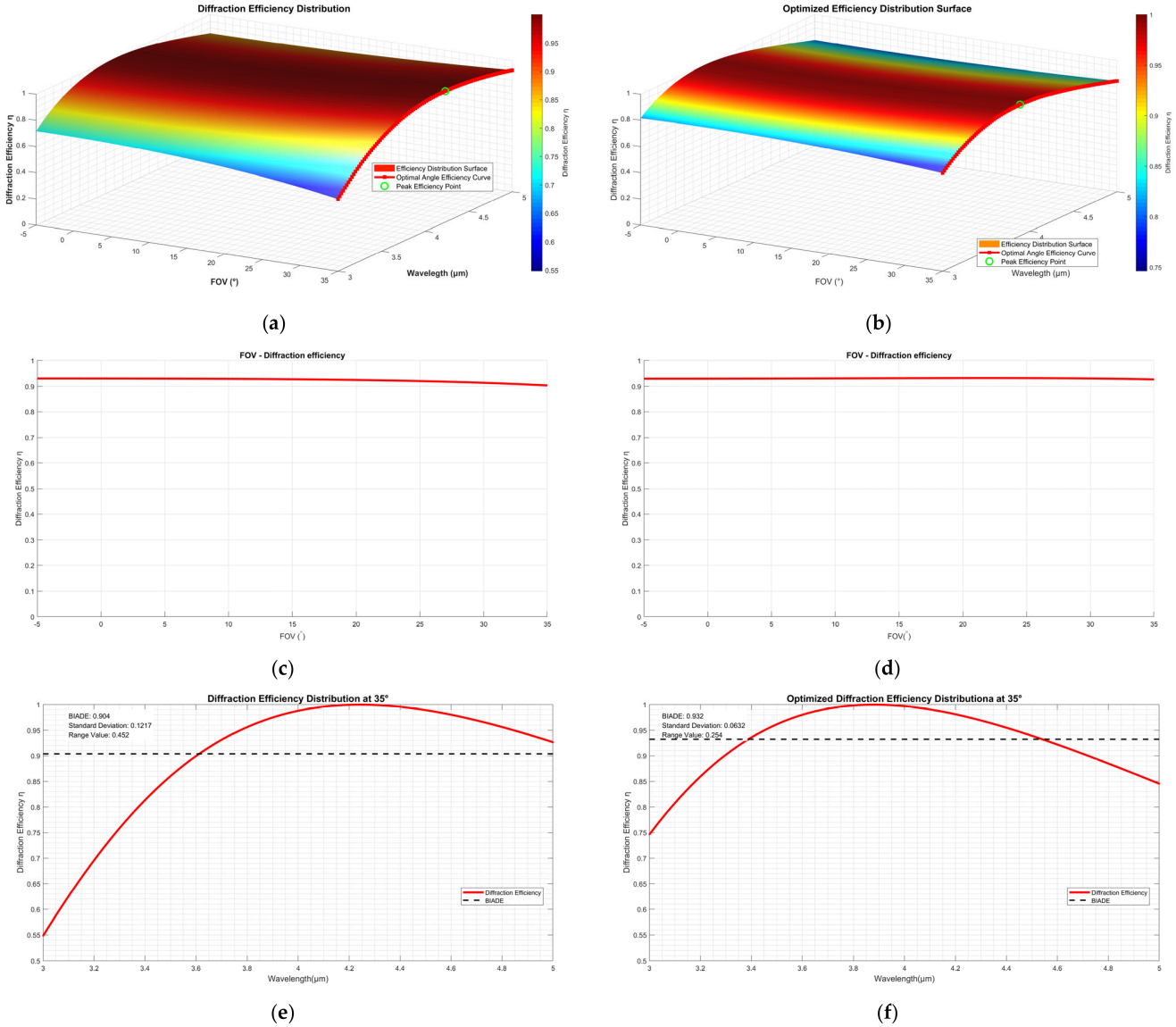


Figure 7. Diffraction efficiency distribution. (**a**) Initial diffraction efficiency distribution at different FOVs and different wavelengths. The red rectangle in the legend are general indications representing the surface of diffraction efficiency distribution; (**b**) optimized diffraction efficiency distribution at different FOVs and different wavelengths. The red rectangle in the legend are general indications representing the surface of diffraction efficiency distribution; (**c**) initial BIADE for different FOVs; (**d**) optimized BIADE for different FOVs; (**e**) initial diffraction efficiency at different wavelengths at 35°; (**f**) optimized diffraction efficiency at different wavelengths at 35°.

Then we optimized the diffraction microstructure of the DFG using the optimization model presented in Section 2.2. In this optimization, the optimization interval for λ_0 is (3.8, 4.2), the optimization interval for α_0 is (10, 20), and the optimization interval for d_0 is (0.75, 0.9). Here, the number of wavelength sampling points S is set to 100. In the convergence objective function f, $b = 1$ and $k = 0.2$. Before optimization, the value of the objective function was $f = 0.085$. After convergence optimization, it is reduced to $f = 0.073$, while the microstructure height is optimized to $d = 0.77$ μm with all other parameters remaining unchanged.

The optimized diffraction efficiency at different FOVs and different wavelengths is calculated and shown in Figure 7b. And the optimized BIADE for different FOVs is shown in Figure 7d, with the value reaching 0.931 for all FOVs. Figure 7f shows the diffraction efficiency at different wavelengths for 35°, with a minimum diffraction efficiency of 0.746, a maximum diffraction efficiency of 1, a range of 0.254, and σ = 0.0632. Accordingly, the range is decreased by 44% and σ by 48%, which demonstrates that the optimized element parameters meet the design requirements.

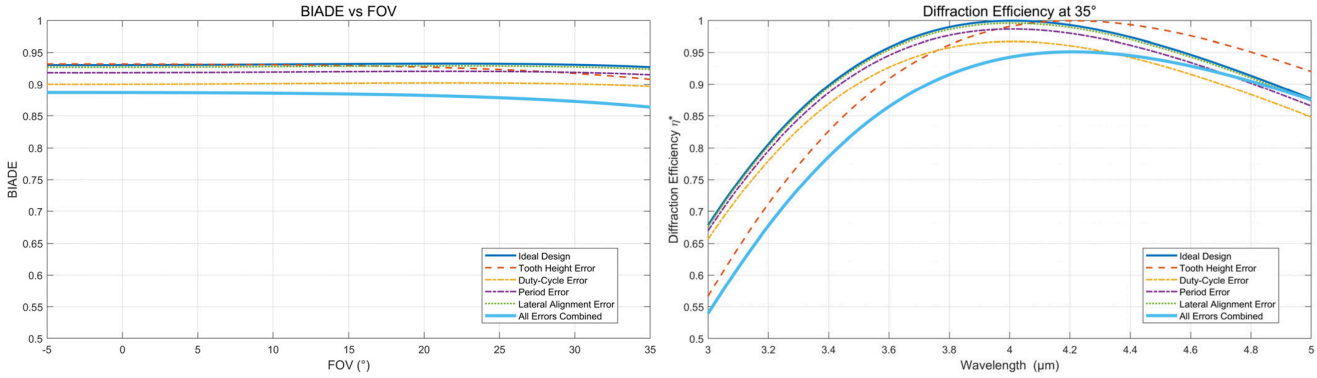
4.2. Tolerance Analysis

Based on several errors summarized in Section 2.3, we added manufacturing errors to the above DFG model. The error values and the corresponding field-averaged BIADE reduction effect are listed in Table 4.

Table 4. Tolerance analysis results.

NO.	Error Name	Value	Loss of $\overline{\eta_m}$
1	Tooth height error	$\Delta d_1 = 5\%$ $\Delta d_2 = 5\%$	0.5%
2	Duty-cycle error	$\Delta f = 5\%$	3.25%
3	Period error	$\Delta T_1 = 1\%$ $\Delta T_2 = -1\%$	1.29%
4	Double-sided lateral alignment error	$\Delta \Phi = 0.2°$ $\Delta y = 1\%$	0.37%
5	All errors combined		5.32%

The BIADEs with various errors for each FOV are shown in Figure 8a. The most significant change in BIADE occurs at 35°, where the ideal BIADE is 0.931 and decreases to 0.864 after adding errors.



(**a**) (**b**)

Figure 8. Tolerance analysis result. (**a**) BIADE with different errors for each FOV; (**b**) the diffraction efficiency variation at different wavelengths after adding errors.

The diffraction efficiency changes at different wavelengths for the 35° FOV after adding errors are shown in Figure 8b, where the diffraction efficiency at each wavelength remains above 0.54. Among these, the tooth height error is 0.04 μm and the period error is 20 μm, both of which can be achieved using existing fabrication processes.

A comparison of the diffraction efficiency for each FOV and each wavelength before and after adding errors is presented in Figure 9.

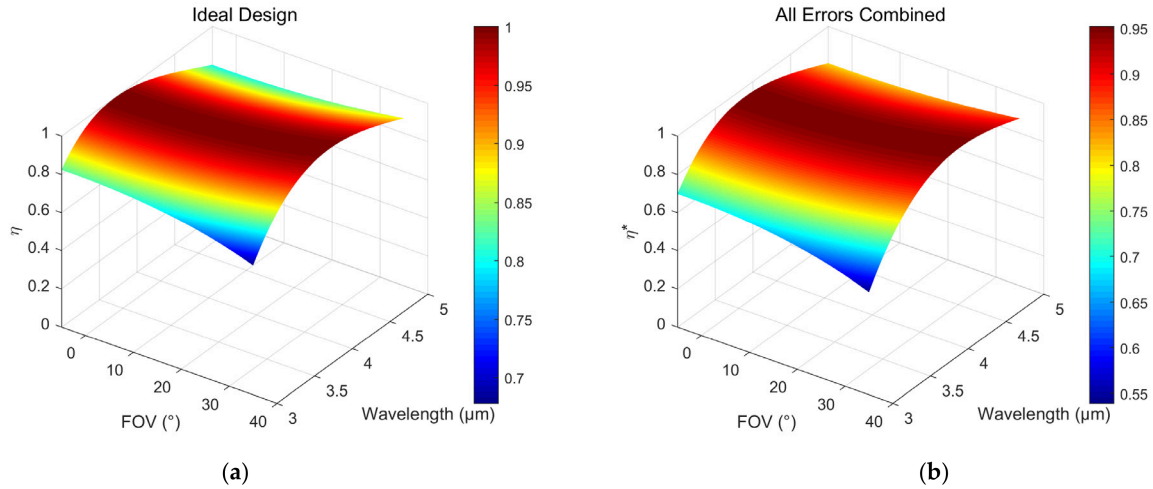


Figure 9. A comparison of the diffraction efficiency distribution. (**a**) The diffraction efficiency distribution for each FOV and each wavelength before adding errors; (**b**) the diffraction efficiency distribution for each FOV and each wavelength after adding errors.

5. Discussion

Based on scalar diffraction theory, we analyze the diffraction process of light rays in the DFG, establish a diffraction efficiency model for the DFG, and propose an optimization method to improve diffraction efficiency over all FOVs while minimizing diffraction efficiency variations across the waveband based on a convergent objective function. Using this method, two DFG designs for beam deflection in the 3–5 μm waveband with 4° and 40° instantaneous FOVs were completed. After optimization, the BIADE of two DFGs was increased to above 0.93, and the standard deviations of the bandwidth diffraction efficiency were reduced by 23.5% and 48%. The design results demonstrate that this method can effectively guide the design of DFG diffractive microstructures.

Furthermore, based on tolerance analysis model, we performed tolerance analysis on the designed DFGs. The results indicate that, after adding fabrication errors, the BIADE of both elements across all FOVs can exceed 0.86, maintaining a high diffraction efficiency.

The optimization design method proposed in this paper supplements the research on DFG diffractive microstructure design and diffraction efficiency analysis, providing theoretical support for advancing the practical fabrication and application of DFGs. In future work, we will focus on the practical fabrication of DFGs, conduct chromatic aberration analysis and diffraction efficiency analysis on the manufactured elements, and further refine the design optimization model.

Author Contributions: Conceptualization, N.X., J.C. and J.F.; methodology, N.X. and Y.W.; formal analysis, N.X., B.X. and N.M.; investigation, N.X., J.F., Y.W. and N.M.; resources, N.X., B.X. and Y.W.; data curation, J.F. and Y.W.; writing—original draft preparation, N.X.; writing—review and editing, J.C., Y.W. and N.M.; visualization, N.X.; supervision, J.F.; project administration, J.C. and J.F.; funding acquisition, J.C. All authors have read and agreed to the published version of the manuscript.

Funding: This research was funded by Opening Funding of the National Key Laboratory of Electromagnetic Space Security, grant number JCKY2024240C006.

Data Availability Statement: Data are contained within the article.

Acknowledgments: We would like to express our gratitude to the National Key Laboratory of Electromagnetic Space Security for providing technical assistance.

Conflicts of Interest: The authors declare no conflicts of interest.

References

1. Rosell, F.A. Prism scanner. *J. Opt. Soc. Am.* **1960**, *50*, 521–526. [CrossRef]
2. Huang, F.; Ren, H.; Wu, X.Y.; Wang, P.F.I. Flexible foveated imaging using a single Risley-prism imaging system. *Opt. Express* **2021**, *29*, 40072–40090. [CrossRef] [PubMed]
3. Li, A.; Liu, X.; Gong, W.; Sun, W.; Sun, J. Prelocation image stitching method based on flexible and precise boresight adjustment using Risley prisms. *J. Opt. Soc. Am.* **2019**, *36*, 305. [CrossRef] [PubMed]
4. Li, C.C.; Yang, H.T.; Ma, Y.J.; Cai, W.X. Design of an infrared/laser dual-band common-aperture optical system based on harmonic diffraction. *Appl. Opt.* **2026**, *65*, 1983–1993. [CrossRef] [PubMed]
5. Li, C.X.; Fan, H.; Gao, B.; Chen, Y.W.; Yu, W.X. Efficient hybrid aberration spatial-calibrated 3D network for liquid-lens-based diffractive spectral imaging. *Opt. Express* **2026**, *34*, 3702–3712. [CrossRef] [PubMed]
6. Safeer Sadiq, M.; Qureshi, H.S.; Ullah, S.; Ghafoor, F. Coherence-controlled azimuthal modulation of atomic ensemble susceptibility, grating, and Fraunhofer diffraction. *Opt. Express* **2025**, *33*, 53919–53936. [CrossRef] [PubMed]
7. Xiong, J.H.; Wang, Z.J.; Wang, Y.T. Eliminating chromatic aberrations of diffractive lenses in varifocal virtual reality displays. *Photonics Res.* **2025**, *13*, 3466–3475. [CrossRef]
8. Chen, C.W. Grism (Grating-Prism Combination). U.S. Patent 5,652,681, 29 July 1997.
9. Chen, C.W. Achromatic and Apochromatic Prism Element Employing Prisms and Grating. U.S. Patent 5,625,499, 29 April 1997.
10. Weber, D.C.; Trolinger, J.D.; Nochols, R.G.; Lal, A.K. Diffractively corrected Risley prism for infrared imaging. *Proc. SPIE* **2000**, *4025*, 79–86.
11. Missig, M.D.; Morris, G.M. Diffractive optics applied to eyepiece design. *Appl. Opt.* **1995**, *34*, 2452–2461. [CrossRef] [PubMed]
12. Chen, C.W.; Anderson, J.S. The use of diffractive optical element in 3-5 micrometer optical system. *Proc. SPIE* **1993**, *2015*, 1–13.
13. Jannson, T.; Aye, T.M.; Savant, G. Dispersion and aberration compensation techniques in diffractive optics and holography. *Proc. SPIE* **1994**, *2152*, 44–70.
14. Chen, C.B. Beam steering and pointing with counter-rotating grisms. *Proc. SPIE* **2007**, *6714*, 671409.
15. Nie, X.; Yang, H.F.; Xue, C.X. Diffractively corrected counter-rotating Risley prisms. *Appl. Opt.* **2015**, *54*, 10473–10478. [CrossRef] [PubMed]
16. Xie, N.; Chang, J.; Xie, B.Q. Design of a wide-field deflection system using a self-achromatic grism. *Photonics* **2025**, *12*, 1178. [CrossRef]
17. Xue, C.X.; Cui, Q.F. Design of multilayer diffractive optical elements with polychromatic integral diffraction efficiency. *Opt. Lett.* **2010**, *35*, 986–988. [CrossRef] [PubMed]
18. Xue, C.X.; Cui, Q.F.; Liu, T.; Yang, L.; Fei, B. Optimal design of a multilayer diffractive optical element for dual wavebands. *Opt. Lett.* **2010**, *35*, 4157–4159. [CrossRef] [PubMed]
19. Mao, S.; Lai, T.; Nie, H.L. Optimal design and application of double-layer diffractive optical element over wide temperature range. *Acta Opt. Sin.* **2023**, *43*, 0822026.
20. Zhao, L.D. *Studies on Design Theory and Application of Multilayer Diffractive Optics*; Changchun University of Science and Technology: Changchun, China, 2019.

Disclaimer/Publisher's Note: The statements, opinions and data contained in all publications are solely those of the individual author(s) and contributor(s) and not of MDPI and/or the editor(s). MDPI and/or the editor(s) disclaim responsibility for any injury to people or property resulting from any ideas, methods, instructions or products referred to in the content.